Undulations and fluctuations in a lamellar phase lyotropic liquid crystal and their suppression by weak shear flow

A. Lutti and P. T. Callaghan*
MacDiarmid Institute for Advanced Materials and Nanotechnology, School of Chemical and Physical Sciences, Victoria University of Wellington, New Zealand
(Received 10 August 2005; published 26 January 2006)

Using multi-echo pulsed gradient nuclear magnetic resonance (NMR) we measure the anisotropic diffusion of water molecules in the lamellar phase of lyotropic system composed of cetylpyridinium chloride/hexanol diluted in brine. The technique reveals the Fourier spectrum of the molecular velocity autocorrelation function, and its repetitive compensating nature permits effective measurement in the presence of shear flow. We show that under zero shear the phase is highly oriented and that both the amplitude and fluctuation correlation time of lamellar undulations can be measured. The suppression of undulations by weak shear is apparent. We further measure transverse lamellae permeability arising from defects.

DOI: 10.1103/PhysRevE.73.011710 PACS number(s): 61.30.St, 87.16.Dg, 68.35.Fx

I. INTRODUCTION

The naive picture of a lamellar phase lyotropic liquid crystal, formed from amphiphiles in water, is that of a periodic stack of planar bilayers separated by solvent molecules. Ideally, the system forms a highly ordered smectic phase, with a well-defined lamellar spacing (on the order of 10 nm) and a well-defined local director. Deviations from ideality include structural defects and orientational deviations (undulations) in the lamellae. At a local level bilayers will exhibit fluctuating (Helfrich) undulations. Collision of such undulations in adjacent bilayers results in an entropy decrease and consequential rise in free energy. Nonionic surfactants stabilize mainly by steric interactions while for ionic surfactants, electrostatic interactions play a role in bilayer dynamics.

The effect of shear flow on lyotropic lamellar systems has been the subject of recent interest. In most complex fluids, provided that the deformation rate is higher than some characteristic mesophase relaxation rate, shear flow may induce structural re-organization [1–3]. For lyotropic lamellar systems, shear may influence director orientation. In particular, at low deformation rates, shear flow characteristically induces lamellar orientation [4–6], most commonly with lamellae directors oriented along the velocity gradient direction (parallel direction or so-called "c-orientation"). Furthermore, evidence from light scattering studies suggests that shear can reduce defects in the lamellar structure [7], and decrease the lamellar spacing [8]. When subject to higher shear rates ($\sim 1\ s^{-1}$) these lamellar phases tend to reorganize to form spherical multi lamellar vesicles (MLV), the transition occurring at a critical shear-rate value that depends on the interlayer spacing [9], presence of defects [10,11], and salinity [7,12]. The size of these spherical vesicles is known to diminish with increasing shear. Further, in some systems a buckling transition to an intermediate structure elongated along the flow direction has been observed [13].

In a two-component liquid, shear flow may induce instabilities since shear-induced elastic stress gradients can oppose the chemical potential gradients which normally drive the relaxation of concentration fluctuations, thus enhancing the amplitude of those fluctuations ("Reynolds effect") [14] although shear flow can also act to suppress the amplitude of fluctuations, through elastic deformation causing an increase in energy cost associated with the fluctuation formation ("Maxwell effect") [14]. While these effects compete, they affect different length scales on the system [14]. In lyotropics, the Maxwell effect is expected to have most influence for wavelengths above 1×10^3 nm while the Reynolds effect acts on shorter wavelengths. Zilman and Granek [15] have suggested that the lamellar to onion transition may result from a shear-induced instability, which arises from the excess area resulting from the suppression of the thermal fluctuations by a coupling with the flow (Maxwell effect). This excess area has the effect of creating a lateral pressure through the shearing gap and therefore leads to the buckling of the whole stack.

To date, there have been few reports concerning the effect of weak shear on lamellar fluctuations. Al Kahawaji *et al.* [7] showed by dynamic light scattering that shear suppresses undulation fluctuations, leading to a dependence of bending elasticity modulus on shear rate. Below a minimum shear rate, on the order of $1\ s^{-1}$, the light scattering autocorrelation functions were no longer simple exponential decays, an effect which they attribute to lamellar phase defects being removed under shear flow. In the present work, our focus is on shear values well below that required for onion formation. In particular we are concerned to measure the impact of weak shear on membrane undulations. We here examine an ionic surfactant system, the amphiphilic bilayer lamellar phase cetylpyrydinium chloride and hexanol diluted in brine. Our measurements are carried out both in equilibrium and under weak shear, that is, at low Deborah number. In doing so we have chosen to work, in narrow gap cylindrical Couette cell geometry, using a lyotropic system which forms, in equilibrium, a highly ordered lamellar phase in the c-orientation, with the lamellar directors normal to the wall surface. The object of the present study is to first determine the degree of equilibrium orientation of the phase. We argue that our sys-

*Email address: paul.callaghan@vuw.ac.nz

tem is highly oriented in equilibrium, and that rather than co-existing with other domains of perpendicular alignment, these c-oriented domains show small angle orientational undulations. We set out to examine the undulation structure and dynamics and seek to observe how that structure changes at very low shear rates.

The principal mode of examination chosen in the present work is the measurement of water molecule self-diffusion, in different directions, using pulsed gradient spin echo (PGSE) NMR, a method which is well-adapted to the study of topological characteristics in lyotropic liquid crystals. This PGSE NMR technique, we have further developed, such that the gradient pulses are applied in rapid succession in a multi echo train. The advantage of such an approach is twofold. First, it allows us to measure the diffusion spectrum, $D(\omega)$, of water molecules, giving us (indirect) access to the frequency domain of fluctuations down to times, relatively short on the timescale of usual PGSE NMR diffusion measurements, i.e., less than 10 ms. Second, the repetition of gradient pulse pairs of opposite-signed displacement encoding means that dispersion due to shear is compensated, allowing us to perform accurate measurements of diffusion under shear flow. It is important to note that our NMR method reveals displacements of much longer range than the bilayer spacings. In consequence we are not directly sensitive to fluctuations of individual lamellae. As we shall show, the NMR measurements of $D(\omega)$, do, however, reveal distinctive equilibrium bilayer undulations which are strongly suppressed by even the smallest shear rate used, $0.002\ s^{-1}$, but leaves unaffected fluctuation modes with low Deborah number. Characteristic bilayer fluctuation times suggested by the $D(\omega)$, measurements are compared with those observed by dynamic light scattering. We further measure diffusive permeation by water molecules across the bilayers.

II. THEORY

The details of the multi-echo PGSE NMR methodology can be found elsewhere, and technical aspects of particular relevance to Rheo-NMR will be presented in another article. For clarity however, we here briefly describe the NMR methodology. We then introduce the essential physics behind the use of molecular self-diffusion to look at bilayer defect structure.

We will demonstrate that the lyotropic liquid crystal lamellae studied here are highly oriented with their directors normal to the Couette cell surfaces. This has particular consequences for the diffusion of water molecules in the intervening layers. In particular diffusion is relatively free along the tangential (x) direction and the longitudinal (z) direction. However, in that radial (y) direction, diffusion is strongly impeded at length scales greater than the interlamellar spacing ($\sim$10 nm). Since all PGSE NMR diffusion measurements performed here are only sensitive to distances well in excess on this distance, diffusion normal to the bilayers will only be observed under three conditions. The first is that the bilayers are deformed due to static undulations, which allows a component of the free diffusion in the x-z plane between the layers to be projected along the y axis. The second is that undulations may fluctuate, carrying water molecules with them in their y displacements. The third is that the lamellae contain defects which permit permeation of water molecules from layer to layer. All these effects will be apparent in this work.

We will here develop a model for such processes in the terms of the anisotropic diffusion experiments which we have carried out. First, however, we describe the theory of multi-echo PGSE NMR, showing how time-dependent diffusive displacements influence the amplitude of the measured echo attenuations.

A. Multi-echo PGSE NMR and the diffusion spectrum

The fundamental element of the PGSE NMR method is the application of two (oppositely signed) magnetic field gradient pulses of equal amplitude, g, and duration δ, separated by an "observation time" Δ. This results in the labeling of the (water molecule proton) spins with a phase proportional to the gradient amplitude and duration and to the change of position of the water molecules between the time of application of the two pulses. Provided that this motion is purely self-diffusive, the attenuation of the resulting spin-echo signal amplitude can be used to determine the mean-squared displacement of water molecules over the time Δ.

In the case of shear, however, the spin phases contain a contribution arising from the inhomogeneous flow, so that dispersive contributions to the echo amplitude may dominate. This effect can be removed by repeating the pair of encoding gradients, but with inverted effective polarities (Fig. 1). The flow contribution to the overall displacement is then compensated leaving only the contribution of the irreversible displacements due to diffusion untouched [16]. In our case of a rotating flow field an efficient flow compensation requires short time delays between gradient pulses so that the direction of the velocities can be considered constant. But this restriction gives little time between the pulses for the spins to diffuse, leading to difficulties in the estimation of the diffusion coefficient. However, by successive repetition of the compensated gradient pulse pairs, sufficient attenuation may be achieved for accurate diffusion coefficient determination. The pulse sequence is shown in Fig. 1.

The multi-echo PGSE NMR experiment has been demonstrated and analyzed by Callaghan and Stepisnik [17], and used in a number of applications [18–20]. The multi-echo train imparts successive attenuations to the echoes, and is sensitive to the details of the diffusive process through the periodic excursions of the spin phases caused by the successive, oppositely signed, gradient pulse pairs. The effect is best analyzed in the frequency domain of the motion, using the frequency characteristics of the gradient pulse train. For a long train of many pulse pairs, the train has narrow spectrum of characteristic frequency $1/T$, where T is the repetition period of the gradient time integral. In particular [17]

$$E(t) = \exp\left(-\frac{\gamma^2}{2\pi} \int_{-\infty}^{\infty} D_{\alpha\alpha}(\omega) |F(\omega)|^2 d\omega \right) \qquad (1)$$

where

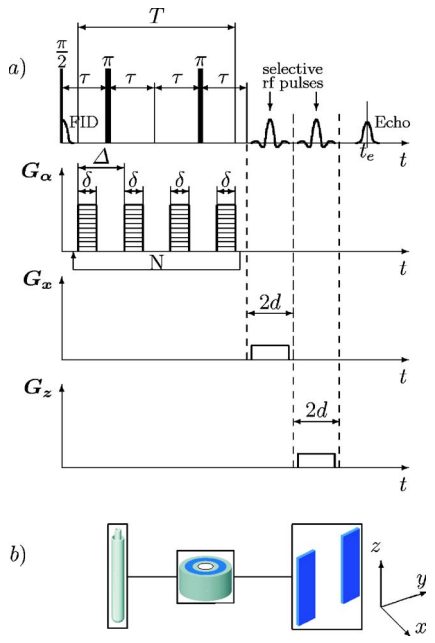

FIG. 1. (Color online) (a) Multi pulsed gradient spin echo experiment in which a repetitive train of repeated four diffusion-encoding gradient pulses is followed by slice selective rf/gradient pulse combinations. Note that the two pairs of gradient pulses depicted have opposite effective sign for motion encoding. The diffusion-encoding gradient, G_α, may be applied along any of the Cartesian axes. (b) Selective excitation enables measurement on a chosen slice.

$$F(\omega) = \int_0^\infty F(t)e^{-i\omega t}dt \tag{2}$$

and

$$F(t) = \int_0^t g^*(t')dt' \tag{3}$$

The diffusion spectrum, in this context, is simply the Fourier transform of the molecular velocity autocorrelation function [21]

$$D_{\alpha\alpha}(\omega) = \int_0^\infty \langle v_\alpha(t)v_\alpha(0)\rangle e^{-i\omega t}dt \tag{4}$$

where α is one of the (chosen) axis directions, x, y, or z.

Equation (1) indicates that the experiment is sensitive to the region of the diffusion spectrum sampled by the frequency characteristic of the gradient sequence. More precisely, for an N-period multi-echo train,

$$|F(\omega)|^2 = \left(\frac{2\gamma G\delta}{\omega}\right)^2 \frac{\sin^2(N\omega T/2)}{\cos^2(\omega T/4)} \sin^2(\omega T/8) \tag{5}$$

The essential features of Eqs. (1) and (5) are shown in Fig. 2. It consists of one main lobe centered at $\omega=2\pi/T$. It is therefore possible to measure the diffusion spectrum of the system by appropriately varying the period of the NMR sequence. Of course, the frequency dependence of the diffusion spectrum to be studied depends on the details of molecular

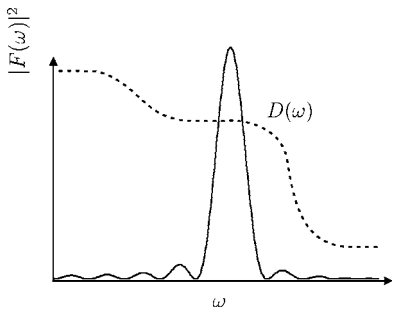

FIG. 2. Schematic effective gradient spectrum $|F(\omega)^2|$ used to sample the diffusion spectrum, $D(\omega)$. The effective gradient, $g^*(t)$, comprises a train with a characteristic period T so that $\omega=2\pi/T$.

displacement fluctuations in the system under study. For modeling purposes, we may derive the velocity autocorrelation function, and hence, $D_{\alpha\alpha}(\omega)$ from a knowledge of the mean-squared displacements, $\sigma^2_{\alpha\alpha}(t)=\langle(x_\alpha(t)-x_\alpha(0))^2\rangle$, i.e.

$$\langle v_\alpha(t)v_\alpha(0)\rangle = \frac{1}{2}\frac{\partial^2\sigma^2_{\alpha\alpha}(t)}{\partial t^2} \tag{6}$$

B. Model for diffusion between undulating lamellae

Figure 3 shows a schematic representation of the lamellar morphology in the Couette cell in the "c" orientation. Water molecule diffusion in the x and z directions is relatively unimpeded. By contrast, diffusion in the radial (y) direction will give an indication of defect-related permeability as well as orientational deviations of the lamellae from pure x-z orientation. In this section we will be concerned to calculate the radial element of the diffusion tensor, $D_{yy}(\omega)$.

In Fig. 3 we depict undulation morphology, characterized by an amplitude u_m, wavenumber k_m, and fluctuation corre-

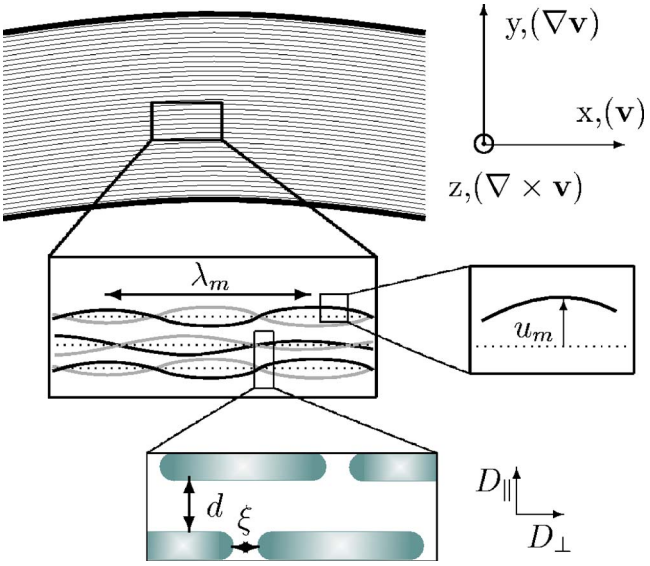

FIG. 3. (Color online) Lamellar system in the "c orientation." Note that pore defects allow some permeation of water in the direction normal to the lamellae. Gray and black represent the same bilayers at different times.

lation time τ_m. The spacing between the layers is d, leading to a characteristic diffusion time, τ_d, on the order of d^2/D_0. Water molecules diffusing in the interlamellar layer will, for times in excess of τ_d, be confined to two-dimensional diffusion. Such diffusion ($D_\perp$), for the undulations shown here, converts x displacements into y displacements. Furthermore, undulation fluctuations will carry the water molecules, providing an additional mechanism for radial movement. Allowing the inter-lamellar layer displacement to be expressed in terms of a sum of modes we write, for the case $t \gg \tau_d$

$$y(t) = \sum_m u_m \cos(k_m x(t) + \phi_m(t)) \tag{7}$$

where $\phi_m(t)$ is the phase factor which describes membrane fluctuations. Allowing for diffusion along x we find for $\Delta y(t) = y(t) - y(0)$

$$\Delta y(t) = 2\sum_m u_m \sin\left(k_m \frac{\bar{x}}{2} + \frac{\bar{\phi}_m}{2}\right)\sin\left(k_m \frac{\Delta x(t)}{2} + \frac{\Delta \phi_m(t)}{2}\right) \tag{8}$$

where $\bar{x}$ and $\bar{\phi}_m$ are the mean values. Assuming that the mode phases are uncorrelated, and that there is no correlation between the mean phase and positions and their displacements $\Delta x(t)$ and $\Delta \phi_m(t)$ one obtains

$$\langle \Delta y(t)^2 \rangle = 2\sum_m u_m^2 \left[\left\langle \sin^2\left(k_m \frac{\Delta x(t)}{2}\right)\right\rangle + \left\langle \sin^2\left(\frac{\Delta \phi_m(t)}{2}\right)\right\rangle - \left\langle \sin^2\left(k_m \frac{\Delta x(t)}{2}\right)\right\rangle \left\langle \sin^2\left(\frac{\Delta \phi_m(t)}{2}\right)\right\rangle \right] \tag{9}$$

Assuming Gaussian displacements $\Delta x(t)$ along the flow direction (i.e., in $D_\perp$), $2\langle \sin^2(k_m[\Delta x(t)/2])\rangle$ reduces to $1 - \exp(-k_m^2 D_\perp t)$ and the radial mean squared displacement becomes

$$\langle \Delta y(t)^2 \rangle = \sum_m u_m^2 \left(1 - \exp\left(-\frac{t}{\tau_m'}\right)\right) \tag{10}$$

where $1/\tau_m' = 1/\tau_m + k_m^2 D_\perp$. Note that the rate $k_m^2 D_\perp$ arises directly from the effect of the $\langle \sin^2(k_m[\Delta x(t)/2])\rangle$ term while the rate $1/\tau_m$ arises from the term $\langle \sin^2(\Delta \phi_m(t)/2)\rangle$ in Eq. (9). A similar exponential term may be derived for the transition from free three-dimensional diffusion at times $t \ll \tau_d$ to the diffusion apparent at $t \gg \tau_d$. Taking the second derivative to obtain the velocity autocorrelation function, then Fourier transforming, one obtains a sum of Lorentzian spectral terms,

$$D_{yy}(\omega) = D_0 L(\omega, \tau_0) - D_0 L(\omega, \tau_d) + \frac{1}{2}\sum_m u_m^2 \left(\frac{1}{\tau_m'} L(\omega, \tau_d) - \frac{1}{\tau_m'} L(\omega, \tau_m')\right) \tag{11}$$

where $L(\omega, \tau) = (1 + \omega^2 \tau^2)^{-1}$ and τ_0 is the molecular collision time. In the limit $t \gg \tau_d$ applicable to the present study, we may write

$$D_{yy}(\omega) = \frac{1}{2}\sum_m u_m^2 \frac{1}{\tau_m'}\left(1 - \frac{1}{1 + \omega^2 \tau_m'^2}\right) \tag{12}$$

By varying the gradient pulse spacing frequency ω we can probe the spectrum. Notice that the characteristic time τ_m' will be set by either the undulation fluctuation rate $1/\tau_m$ or the diffusive rate $k_m^2 D_\perp$ depending on which is dominant. Our NMR approach is unable to distinguish between the separate dynamic contributions of membrane fluctuations and diffusive excursions of water molecules along the bilayers. Independent light-scattering measurements, which pick up bilayer fluctuations alone do, however, provide a complementary check.

III. EXPERIMENT

The system studied here is 30% w/w cetylpyridinium chloride and hexanol diluted in brine (1% w NaCl). All materials were purchased from Sigma-Aldrich. The role of the NaCl is to screen the Debye interactions between these ionic surfactants so that the stabilization of the lamellae is expected to occur via their fluctuations (Helfrich phase). Samples were prepared at room temperature and allowed to equilibrate for one week before use. The mass ratio hexanol/CpCl is taken from the phase diagram [22] and at 0.92 is designed to provide a lamellar phase remote from any phase boundaries. Using the relative density of hexanol (0.8136) taking the relative density of CpCl to be around unity of water, we therefore find that the volume fraction of surfactant and co-surfactant is $\Phi_m = 0.32$

All measurements were carried out using a Bruker Avance 300 MHz NMR spectrometer, using the three-axis magnetic field gradients of the Micro2.5 probe.

The interlayer spacing for this system can be estimated using the relation [13]

$$d(\dot{A}) = \frac{a - bln(\Phi_m)}{\Phi_m} \tag{13}$$

where Φ_m is the volume fraction of surfactant and co-surfactant. Using the data of Porcar *et al.* for the dependence of layer spacing d on membrane volume fraction in lamellar CpCl/hexanol/brine, we obtain $a = 2(0.5)$ and $b = 0.4(0.2)$, leading to a interlayer spacing $d \sim 8$ nm for our system.

Shear is applied using a Couette cell made of two concentric glass NMR tubes of 16 mm (O.D) and 18 mm (I.D), respectively. The Couette cell vorticity axis is aligned parallel to the (vertical) direction of the polarizing magnetic field. After slowly pouring the sample into the outer tube, the inner one is then slowly inserted. The system is then heated at a temperature of 60 deg for half an hour so as to eliminate any orientational effect due the pre-shearing of the lamellae during Couette assembly. For Rheo-NMR work, the inner cylinder can be rotated within the NMR spectrometer by means of a specially constructed shaft and stepper-motor-gearbox drive. Knowing the critical importance of the salinity in determining the delay time before reaching a steady state [12], a shearing period of $1\frac{1}{2}$ hours was allowed before NMR measurements were performed.

In our experiment we wish to select a small arc of the Couette cell so that the velocity and gradient directions are well-defined. This is achieved by means of two "slice-selective" radiofrequency pulses applied in combination with magnetic field gradients. These slice-selective pulses come at the end of the multi-echo train designed to encode the nuclear magnetization with diffusion information. One slice (thickness 30 mm) is taken perpendicular to the longitudinal (vorticity) axis of the couette cell and defines the longitudinal section to be averaged. The other slice (thickness 3 mm) is taken perpendicular to a diametral direction. This choice of selected sample volume defines a simple three-dimensional cartesian system along which one can apply the diffusion-encoding gradients. These Cartesian then correspond to the directions x [tangential=velocity direction ($\mathbf{v}$)], y [radial =velocity gradient direction ($\nabla\mathbf{v}$)], and z [longitudinal =vorticity direction ($\nabla\times\mathbf{v}$)].

In all diffusion experiments the NMR signal was detected using the proton nucleus of water molecules. For some experiments however, deuteron NMR was used to check the orientational alignment. For these latter experiments samples were prepared using D_2O rather than pure H_2O.

IV. DEUTERIUM NMR SPECTROSCOPY OF INTER-LAMELLAR WATER

We first report on the results of a deuterium NMR study of lamellar orientation. As spin-1 nuclei, deuterons are sensitive to the surrounding electric field gradients whose symmetry axis is determined by the local molecular orbital. That interaction, which acts as a first order perturbation to the dominant magnetic (Zeeman) interactions of the spins, is projected along the magnetic field direction through the second-rank Legendre polynomial $P_2(\cos\theta)$ where θ is the angle between the bond axis and the field. In the isotropic liquid state the tumbling of D_2O molecules would tend to average this projection to zero. However, in a lamellar phase, some inherited, motionally averaged order remains as a result of collision with the bilayers. For a unique bilayer orientation the deuteron resonance line is split in two, that splitting providing a relative measure of the averaged value, $P_2(\cos\theta)$. A system of bilayers oriented with its director parallel to the field will exhibit a quadrupole splitting twice that a system with perpendicular orientation.

Figure 4 presents the resulting ^2H spectrum of a lamellar phase containing heavy water, in a 1 cm diameter NMR tube as well as inside the 16 mm/18 mm glass Couette cell. Following usual protocols, system had been heated at temperature of 60 deg for half an hour following Couette assembly and the system allowed to equilibrate at room temperature for several days.

Note that the sample in the simple NMR tube shows evidence of a splitting, indicating a preferred orientation. However, there does appear to be a distribution of orientations, as evidenced by the broadened spectrum. By contrast, in the Couette cell case, one notices that the two peaks are quite sharp and well separated, suggesting that the angle orientation of the lamellar bilayers is nearly unique. We shall show, by virtue of our diffusion measurements, that the directors

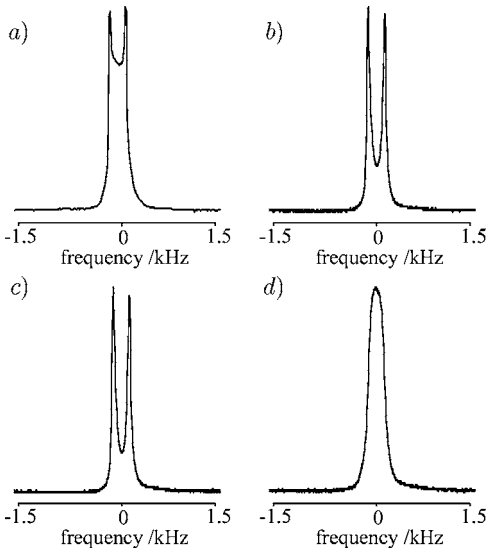

FIG. 4. Deuterium spectrum in (a) a 1 cm diameter NMR tube (b) in the Couette cell $\dot{\gamma}=0\ s^{-1}$, (c) $\dot{\gamma}=1\ s^{-1}$, (d) $\dot{\gamma}=4\ s^{-1}$ where a transition to a new mesophase is observable.

are in the velocity gradient ($\nabla\mathbf{v}$) direction. The orientation of the bilayers is most likely induced by the presence of the glass walls. In the case of the 1 mm gap of the Couette cell, the orientation effect is strong, whereas in the 10 mm diameter glass tube, much weaker effect is available to orient the bulk material. The splitting disappears above 4 s^{-1}, indicating a new transition to a new mesophase.

Should some of the bilayers have their directors along the vertical ($\nabla\times\mathbf{v}$) direction, an additional phase with twice the splitting would be apparent. No evidence for this admixed phase is found.

V. DIFFUSION MEASUREMENTS AT ZERO SHEAR

A. Tangential and vertical component

Water diffusion measurements on our equilibrium oriented lamellar phase might be expected to reflect the anisotropy that has been detected by deuterium NMR in the couette cell. The results of the diffusion measurements in the vorticity and tangential directions are shown in Fig. 5. It is clear that the diffusion behavior is identical along these two directions. The unimodal nature of the diffusion distributions is illustrated by the linear attenuation on the semi-logarithmic plot of *log(echo amplitude)* vs $\gamma^2g^2\delta^2 2N(\Delta-\delta/3)$.

The value of the diffusion coefficient obtained, close to that of the free diffusion of water ($D=1.6\times10^{-9}\ m^2\ s^{-1}$) indicates that solvent molecule diffusion is little perturbed by the presence of the lamellae. The rms displacements undertaken by the water molecules during the echo train here are on the order of 50 μm. This free diffusion supports our contention that the bilayers are oriented with directors normal to the walls of the Couette cell, throughout the sample, i.e., along the radial direction, leaving the tangential and vertical directions equivalent. We note that no deviation from linearity is apparent in Fig. 5 down to the 10% attenuation level.

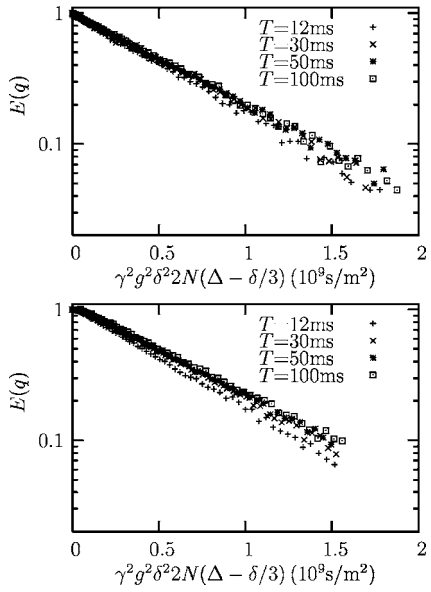

FIG. 5. Attenuation of the echo train signal, gradients applied along tangential and vertical directions, for several values of the gradient waveform period T.

This data, taken together with the deuterium NMR spectrum, suggests that there is no significant proportion of the sample with lamellar domains in perpendicular orientation, either with directors along the $\nabla \times \mathbf{v}$ or $\mathbf{v}$ directions. In terms of the precision of our measurement, we are able to argue that our system is aligned in the c-orientation ($\nabla \mathbf{v}$) to better than 95%

B. Radial component

A very different behavior might be expected for diffusion along the radial direction. In such a direction the bilayers are expected to strongly inhibit the diffusion of solvent molecules. Because we can only detect displacements much larger than the bilayer spacing, such radial diffusive displacements will only be visible because of (i) permeation through the defects (pores), (ii) angular variations (undulations) projecting part of the diffusion along the bilayers into the radial direction, or (iii) thermal fluctuations of the bilayers transporting the water molecules in the radial direction. If all are present then a multi-mode diffusion might be, therefore, expected.

The experimental results for encoding in the radial direction are shown in Fig. 6. As expected, the echo-attenuation decays are clearly not mono-exponential, and further, exhibit a dependence upon the multi pulse-PGSE period time. Because of the multi-exponential nature of the decay, we choose to analyze this data in two ways. In the first, we take the initial slope, giving us access to the average diffusion coefficient for the particular frequency represented by the preset gradient pulses spacing. This approach leads us to the diffusion spectrum showed in Fig. 7. In the second approach we use inverse Laplace transformation to analyze the various exponential components. As we shall show, such an analysis always reveals a slow mode of decay, whose diffusion coefficient we associate with the permeation of water molecules

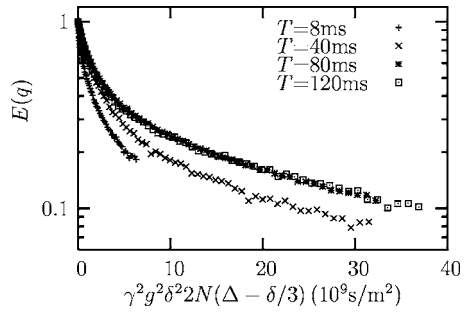

FIG. 6. Attenuation of the echo train signal, gradients applied along the radial direction, for several values of the gradient waveform period T.

across the bilayers. This slow mode represents such a small diffusion coefficient that its inclusion in the "averaging" initial slope analysis is not significant. However, we do in fact remove it to obtain the diffusion spectrum shown in Fig. 7.

Note that the data in Fig. 6 indicate the presence of a fast decay whose contribution is on the order of 50%. We immediately rule out any association of this rapid diffusion with perpendicularly aligned lamellar domains, whose contribution cannot be larger than 5%.

The experimental diffusion spectrum can be fitted with the model described in Sec. V B. A bi-modal behavior fits the data well, yielding similar amplitudes $u_1 \sim 2$ μm and $u_2 \sim 7$ μm but very different characteristic times $\tau_1 \sim 4$ ms and $\tau_2 \sim 100$ ms. At this point we note that in a electrophoretic microrheology investigation of the *n*-dodecyl pentaethyleneglycol monododecylether ($C_{12}E_5$)/1-hexanol/water system, Mizuno *et al.* [23] detected two characteristic fluctuation times that they associated with two characteristic lengths of the system, namely, the distance between two points of collision between two neighboring membranes ($\sim$33 nm, $\sim$170 μs) and the persistence length of the orientational order ($\sim$500 nm, 66 ms). It would be tempting to compare these values with the two characteristic times measured in the present work. However, that associated with the shorter length scale $\sim$33 nm would not be measurable using our technique. As we shall show, another explanation is apparent for the $\sim$4 ms time seen.

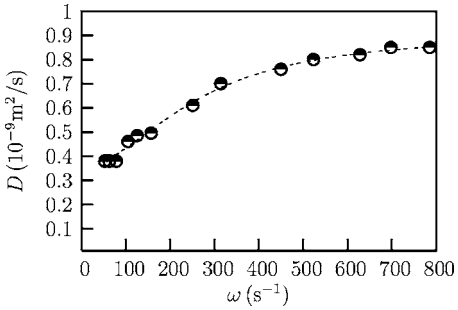

FIG. 7. Diffusion spectrum gradients applied along the radial direction (no shear). The dashed line is a fit using Eq. (12) with two components, i.e., $D(\omega)=(1/2)(u_1^2/\tau_1)(1-1/(1+\omega^2\tau_1^2))+(1/2)\times(u_2^2/\tau_2)(1-1/(1+\omega^2\tau_2^2))$.

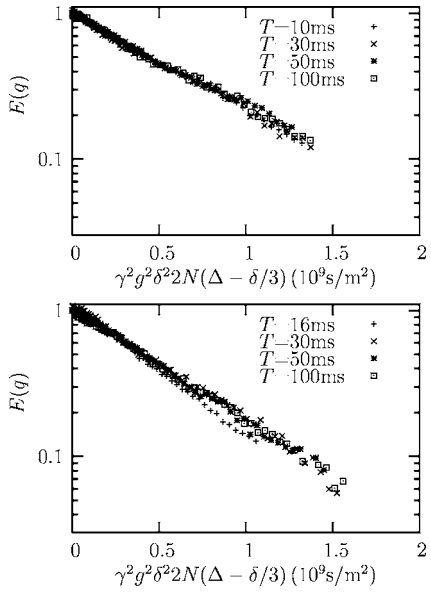

FIG. 8. Attenuation of the echo train signal, gradients applied along the tangential and vertical directions at $\dot{\gamma}=0.02\ \mathrm{s}^{-1}$.

VI. DIFFUSION MEASUREMENTS UNDER SHEAR

A. Tangential and vertical component

The diffusive behavior in the radial, tangential, and longitudinal directions has been examined for a range of low shear rates, from $\dot{\gamma}=0.002\ \mathrm{s}^{-1}$ to $\dot{\gamma}=0.05\ \mathrm{s}^{-1}$. In all these experiments, no significant change was seen for diffusion along the tangential or longitudinal directions (see Fig. 8). We may presume from these results that the director orientation parallel to the $\nabla \mathbf{v}$ direction is maintained. These shear rates are well below the rate required to induce the lamellar to MLV transition ($\sim 2\ \mathrm{s}^{-1}$).

B. Radial component

By contrast, shear appears to have a strong effect on the NMR echo attenuation when the magnetic field gradients are applied along the radial direction. In particular, as shown in Fig. 9, the attenuation now is much weaker than in the nonsheared case, corresponding to a slowing of the diffusion. The changes in the diffusion spectrum can be seen on Fig. 10, for the cases $\dot{\gamma}=0$, 0.002, 0.004, and 0.05 s^{-1}.

Surprisingly, the high frequency plateau is dramatically affected by flow, even at a shear as low as 0.002 s^{-1}. Note

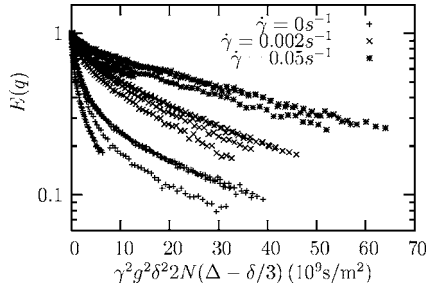

FIG. 9. Attenuation of the echo train signal, gradients applied along radial direction $\dot{\gamma}=0, 0.002, 0.05\ \mathrm{s}^{-1}$.

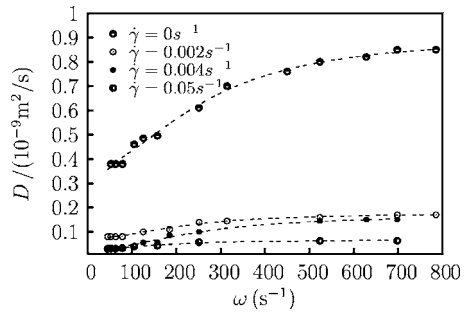

FIG. 10. Diffusion spectrum, gradients applied along the radial direction $\dot{\gamma}=0, 0.002, 0.004, 0.05\ \mathrm{s}^{-1}$. The dashed lines are least square fits using Eq. (12) with two spectral components.

that the fit to the zero-shear diffusion spectrum shows two dominant modes. Paradoxically, it is the faster mode which is severely damped by shear, while the slower mode appears unaffected. However, it is important to note that these diffusive modes may arise either from bilayer fluctuations or from intra-lamellar diffusive excursions of water molecules. If we interpret this phenomenon as the damping of undulations due to the Maxwell effect, then for a Deborah number ~ 1, we require a characteristic time in excess of 100 s, given that this fluctuation mode is affected by such a low shear rate. Such a timescale is much longer than relevant time frames of the NMR pulse sequences so that we may regard these undulations as essentially frozen. The apparent high frequency of the mode therefore arises from water molecule diffusion rather than from undulation fluctuations. In the language of Eq. (12), $\tau_m^{-1} \approx 0$ for this mode and the diffusion spectrum frequency dependence is dominated by the time to diffuse distance k_m^{-1}, on the order of one undulation wavelength.

Our picture is that static undulations in the bilayer director are highly damped by even the lowest shear rate. We now seek to determine their amplitude and wavelength. At zero shear, the rapid inital decay apparent in Fig. 6 represents the enhanced component of the diffusion along the radial direction made possible by projections of the intra-layer diffusion along the radial direction. Fitting the zero-shear data with Eq. (12) we find $(k_m^2 D_\perp)^{-1} = \tau_1 \approx 4$ ms (see Table I). For such a time the characteristic wavelength is $\lambda_1 = 2\pi\sqrt{D_\perp \tau_1} \approx 15\ \mu$m. The amplitude of these undulations is also given by fitting Eq. (12) yielding $u_1 \approx 2\ \mu$m (see Table I). That this value is much less than the wavelength, suggests that angular excursions in the quasi-static undulations are small.

We now turn our attention to the low frequency mode obtained from our fit to the diffusion spectrum, for which $u_2 \sim 7\ \mu$m and $\tau_2 \sim 100$ ms. Unsurprisingly, this mode re-

TABLE I. Amplitudes and frequencies of the fluctuation modes.

$\gamma(\mathrm{s}^{-1})$	$u_1(\mu\mathrm{m})$	$\tau_1(\mathrm{ms})$	$u_2(\mu\mathrm{m})$	$\tau_2(\mathrm{ms})$
0	2(0.1)	3.7(0.4)	7(2)	70(60)
0.002	1(0.1)	4.5(0.6)	5(7)	150(500)
0.004	1(0.1)	4.1(0.8)	1.3(1)	50(100)
0.05	0.7(0.1)	6(2)	3(7)	140(80)

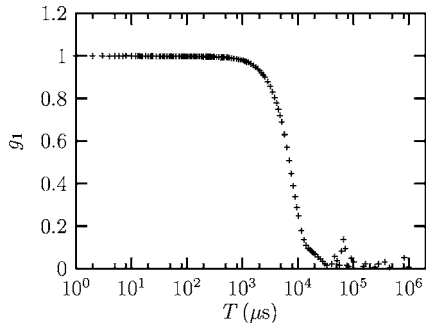

FIG. 11. Correlation function g_1 by dynamic light scattering at an angle $\Theta=15°$.

mains unaffected by shear up to $\dot{\gamma}=0.02\ s^{-1}$ for which $De \ll 1$. This characteristic time is, we believe, associated with fluctuations of the membranes. However, our NMR measurements do not reveal the wavelength associated with this mode. The usual expression of the relaxation rate of an undulation of wavelength $q_\perp$ is [14,24]

$$\tau^{-1} = \frac{K}{\eta} q_\perp^2 \tag{14}$$

where K is the smectic elasticity of the lamellar phase, given by κ/d where κ is the bending elasticity modulus of the bilayers and η is the viscosity.

Al Kahwaji *et al.* [7] have shown that the relaxation of undulation fluctuations can be measured using dynamic light scattering (DLS) provided that the scattering wave vector is

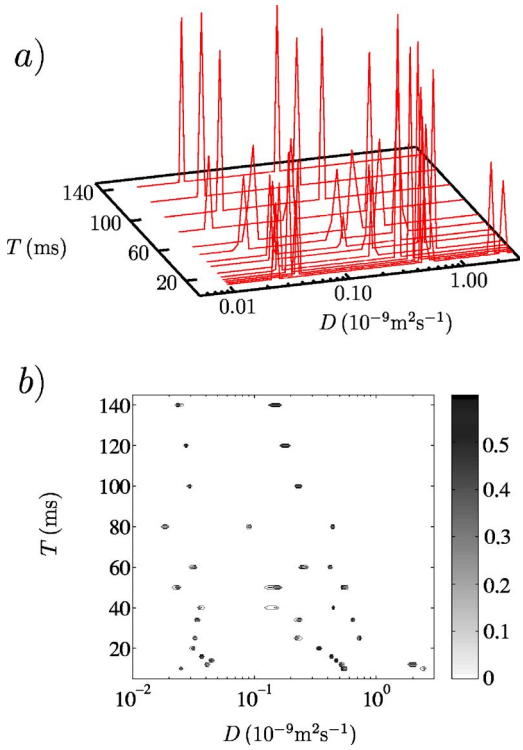

FIG. 12. (Color online) Distribution of radial diffusion coefficients at different waveform periods T. $\dot{\gamma}=0\ s^{-1}$. (a) Stacked profile plot, and (b) intensity map.

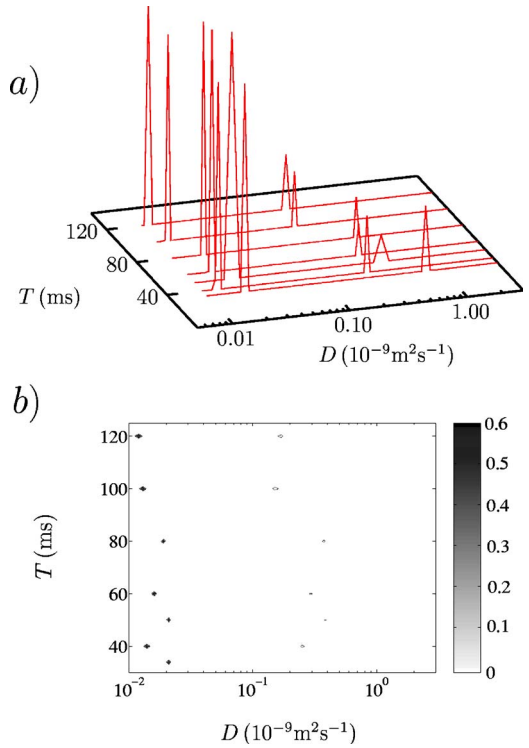

FIG. 13. (Color online) Distribution of radial diffusion coefficients at different waveform periods T. $\dot{\gamma}=0.02\ s^{-1}$. (a) Stacked profile plot, and (b) intensity map.

approximately in the plane of the bilayers. In this case, equation (14) applies and $q_\perp$ corresponds to q. In consequence DLS may be used to obtain an estimate of K/η. Figure 11 shows the result of a DLS experiment carried out in forward scattering geometry ($\Theta=15°$), on our lamellar phase system oriented between two parallel sheets of glass spaced by 1 mm. The incident beam ($\lambda=532\times10^{-9}$ m) is normal to the bilayers, yielding $q=4.1\times10^6\ m^{-1}$ and approximately in the bilayer plane. The time constant of around 10 ms suggests $K/\eta=6\times10^{-12}\ m^2\ s^{-1}$. Using this value we estimate that the wavelength associated with the $\tau_2\sim100$ ms mode measured by NMR, is approximately 5 μm. Notwithstanding the fact that defects can perturb DLS autocorrelation functions measured at zero shear, the rudimentary experiments performed here do give us a rough estimate of the (u_2,τ_2) undulation mode wavelength which is found in the NMR measurements. We find $u_2\approx\lambda_2$, suggesting that the angular excursions for this mode are significantly larger than the quasi-static mode 1. It is also important to note that this second mode measured by NMR may represent an averaged fit to a superposition of undulation fluctuations covering a range of wavelengths.

VII. STUDY OF THE PERMEATION

Of course, as discussed in Sec. V B, permeation of solvent molecules through the membranes is expected to contribute to the overall diffusion along the direction normal to the bilayers. This contribution should be little affected by shear. In order to more carefully examine the shear-dependence of radial diffusion, we analyze each echo attenu-

ation, so as to obtain a diffusion coefficient distribution, by means of inverse-Laplace transformation. Such a distribution of diffusion coefficients provides more detail than the average D value obtained by analyzing the initial behavior of the echo attenuation plots. The results for zero shear and for 0.02 s^{-1} are shown in Figs. 12 and 13. Most of the fast components observable in the zero shear case disappear at 0.02 s^{-1} (Indeed the same effect is also apparent down at 0.002 s^{-1}). The diffusion component which remains has a value of around 3×10^{-11} m^2 s^{-1}, declining to 2×10^{-11} m^2 s^{-1} under shear. We attribute this value to the permeation diffusion coefficient, a permeation which slightly reduces as shear is applied.

It is helpful to consider whether this interpretation of the slow diffusion as arising from permeation is reasonable. One approach is to consider the consequences for the implied number density, n, of pore defects. One approach is to use the model of Constantin and Oswald [25],

$$D_{\parallel} \approx nd^2D_{\perp} \tag{15}$$

It is not our purpose to test the validity of this model here, for example, by carrrying out a systematic study of $D_{\parallel}$ vs d^2, although we would point out that the NMR method we have demonstrated would be ideal for such a study. We may, however, use this relationship to gain some rough estimate of n. For $D_{\parallel}\approx3\times10^{-11}$ m^2 s^{-1} and $D_{\perp}=1.6\times10^{-9}$ m^2 s^{-1} we obtain $n\approx290$ μm^{-2}. Note that our value for $D_{\parallel}/D_{\perp}$ is comparable with that found by Constantin and Oswald [25] in the nonionic $C_{12}E_6$/water system, although with a much smaller interlamellar spacing, their estimate for n was correspondingly larger.

VIII. CONCLUSION

The lamellar phase lyotropic system 30% w/w cetylpyridinium chloride and hexanol diluted in brine (1% w NaCl) exhibits a distinctive c-orientation in the Couette cell, both deuterium NMR and anistotropic diffusion measurements indicating a phase purity of at least 95%. The use of multi pulse gradient spin echo NMR, allows us to scan over the diffusion spectrum associated with displacements normal to the lamellae. These measurements reveal the presence of both fast and slow diffusion modes, which we attribute, respectively, to water diffusion along quasi-static bilayer undulations, and water molecules carried by superposed undulation fluctuations. Under shear, the quasi-static undulations are strongly damped, leaving visible diffusive excursions associated with bilayer fluctuations. All these diffusive motions along the $\nabla\cdot\mathbf{v}$ direction are superposed on a much slower diffusion which we associate with membrane permeability, a permeability which is slightly reduced under shear.

ACKNOWLEDGMENTS

The authors would like to acknowledge grant support from the New Zealand Foundation for Research, Science and Technology and the Royal Society of New Zealand Marsden Fund and Centres of Research Excellence Fund. We are grateful to Allan Raudsepp for assistance with the DLS measurements and their analysis and to Kate McGrath for advice concerning the lyotropic phase used here.

[1] N. A. Clark and B. J. Ackerson, Phys. Rev. Lett. **44**, 1005 (1980).
[2] G. Verstrat and W. Philippo, J. Polym. Sci., Polym. Lett. Ed. **12**, 267 (1974).
[3] D. Roux, in *Theoretical challenges in the dynamics of complex fluids*, edited by T. C. B. McLeish, (Kluwer Academic Publishers, Dordrecht, 1997), p. 203.
[4] O. Diat, D. Roux, and F. Nallet, J. Phys. II **3**, 1427 (1993).
[5] M. Imai, K. Nakaya, and T. Kato, Eur. Phys. J. E **5**, 391 (2001).
[6] S. Muller, C. Borschig, W. Gronski, C. Schmidt, and D. Roux, Langmuir **15**, 7558 (1999); M. Lukaschek, S. Muller, A. Hansenhindl, D. A. Grabowski, and C. Schmidt, Colloid Polym. Sci. **274**, 1 (1996).
[7] A. A. Kahwaji, O. Greffier, A. Leon, J. Rouch, and H. Kellay, Phys. Rev. E **63**, 041502 (2001).
[8] J. Yamamoto and H. Tanaka, Phys. Rev. Lett. **74**, 932 (1995).
[9] S. Ramaswamy, Phys. Rev. Lett. **69**, 112 (1992).
[10] C. Meyer, S. Asnacios, and M. Kleman, Eur. Phys. J. E **6**, 245 (2001).
[11] L. Porcar, G. G. Warr, W. A. Hamilton, and P. D. Butler, Phys. Rev. Lett. **95**, 078302 (2005).
[12] A. Leon, D. Bonn, J. Meunier, A. Al-Kahwaji, O. Greffier, and H. Kellay, Phys. Rev. Lett. **84**, 1335 (2000).
[13] L. Courbin, J. P. Delville, J. Rouch, and P. Panizza, Phys. Rev. Lett. **89**, 148305 (2002).
[14] R. Bruinsma and Y. Rabin, Phys. Rev. A **45**, 994 (1992).
[15] A. G. Zilman and R. Granek, Eur. Phys. J. B **11**, 593 (1999).
[16] P. T. Callaghan, S. L. Codd, and J. D. Seymour, Concepts Magn. Reson. **11**, 181 (1999).
[17] P. T. Callaghan and J. Stepisnik, Adv. Magn. Opt. Reson. **19**, 325 (1996).
[18] P. T. Callaghan and S. L. Codd, Phys. Fluids **13**, 421 (2001).
[19] J. Stepisnik, A. Mohoric, and A. Duh, Physica B **307**, 158 (2001).
[20] J. Stepisnik and P. T. Callaghan, Magn. Reson. Imaging **19**, 469 (2001).
[21] See the discussion on spectral functions, edited by R. Kubo, M. Toda, and N. Hashitsume, *Statistical Physics II* (Springer-Verlag, Berlin, 1978), Sec. 4.3.1.
[22] H. F. Mahjoub, K. M. McGrath, and M. Kleman, Langmuir **12**, 3131 (1996).
[23] D. Mizuno, Y. Kimura, and R. Hayakawa, Phys. Rev. E **70**, 011509 (2004).
[24] F. Nallet, Langmuir **7**, 1861 (1991).
[25] D. Constantin and P. Oswald, Phys. Rev. Lett. **85**(20), 4297 (2000).